RECIPROCATING LUBRICATED SLIDING ON TEXTURED STEEL SURFACES

HENARA L. COSTA, IAN M. HUTCHINGS

Institute for Manufacturing, Department of Engineering, University of Cambridge, UK
ltm-henara@ufu.br, imh2@cam.ac.uk

ABSTRACT: The presence of a lubricant film between two sliding surfaces reduces adhesion and wear. Engineering surfaces can be textured with a uniform micropattern composed of regularly shaped topographical features, which is expected to improve their lubrication. If the surfaces are sliding against each other with a certain velocity and a lubricant fluid is present in the contact, a hydrodynamic film may form spontaneously between them. In lubricated sliding tests of metallic samples, the two conducting samples can be seen as two conductors separated by a lubricant film, which constitute a capacitor if the two samples are insulated from each other. In this work, a bridge circuit was designed where the capacitor created by the two samples and the lubricant film was one of the components of a bridge. The resistors that compose the bridge were selected in order to provide a large range of linear variation between voltage and capacitance, between approximately 50 and 900 pF and the output was a rectified DC voltage signal corresponding to the average of the resultant AC signal for each film thickness. The apparatus was connected to a reciprocating sliding tester with sinusoidal velocity variation in order to achieve regimes of lubrication varying from boundary to hydrodynamic lubrication over the length of the stroke; the velocity varied between zero at the ends of the stroke and 40 mm s^{-1} in the middle. Textured samples containing patterns composed of individual circles and lines were tested using this apparatus. The effects of width and percentage of coverage and of feature orientation were analysed. All the results were compared with those from a standard polished surface.

Key words: surface texturing, surface patterning, thick film lubrication, film thickness, capacitance, reciprocating tests.

1. INTRODUCTION

The texturing of sliding surfaces with regular patterns has received considerable attention as a means of improving their tribological performance. It is a natural development of the more random texturing achieved through processes like abrasive finishing and honing. Three main effects are expected to occur to improve the tribological performance of textured surfaces. The first is the entrapping of wear debris inside the pockets that compose the texture, avoiding their presence between the two surfaces, which could cause abrasive wear [1, 2]. The second is the existence of pockets of lubricant which could be particularly useful in conditions involving high plastic deformation [3]. The third is the enhancement of a hydrodynamic pressure between the surfaces due to the converging wedges constituted by the pockets. The idea of an increased hydrodynamic pressure generated by surface texture started in the 1960's, when Hamilton et al., during the course of their long-term research on parallel rotary-shaft face seals, found evidence of the effect of irregularities on lubrication [4]. Since then, various authors have studied the tribological behaviour of textured surfaces, especially in recent years. These studies include numerical simulations [5-7] and experimental evaluation of textured surfaces [8-10].

However, a better understanding is still needed of the effects on tribological performance of different surface textures. It is necessary to identify, using a more fundamental approach, the effect of each of the variables that define the pattern generated by the texturing process. This work uses a model experimental set-up to investigate the role of surface texturing in generating hydrodynamic pressure in lubricated sliding contacts. The effect of the geometric characteristics of the textures was associated with the increase in film thickness generated by this hydrodynamic pressure.

2. EXPERIMENTAL PROCEDURE

Carbon steel samples with dimensions 35 x 35 x 2 mm were cut from flat plates by electrical discharge machining. Before texturing, the samples were ground and mirror-polished using 1 μm diamond paste. Photochemical etching [11] was then used to texture the surfaces. Although this method might be difficult to apply in an industrial application, due to its cost and complexity, it was regarded as a method that could easily produce textures composed by complex shapes and distributions for the model experiments used in this work. A normal laboratory bench was used for the photolithographic procedure involved in the texturing process. This reduced considerably the complexity and costs of the process in comparison to the use of a clean room. The room was isolated from daylight and yellow illumination was used. The patterns to be generated on the surfaces were designed using Adobe Photoshop® and printed on A4 papers using a laser printer. They were then photographed using an archive microfilm, Kodak ImageLink HQ, to make the masks to be used during the exposure of the resist. This also reduced costs and time that would be involved in the production of conventional metallic masks. A conventional microscope illuminator was used as a UV source for the exposure of the resist and the exposure to UV light was made by contact. Table 1 summarises the conditions used in the photolithographic process. A 10 % nitric acid solution was used to etch the

samples and the depth of the features was varied by changing the etching time.

Table 1. Conditions for photolithographic procedure.

Spinning rotational speed (rpm)	4000
Spinning time (s)	30
Pre-baking temperature (^oC)	95
Pre-baking time (s)	60
Exposure time (s)	300
Developing time (s)	30-60
Developing solution concentration (vol. fraction in water)	1 / 3.5
Post-baking temperature (^oC)	150
Post-baking time (s)	180

The geometrical characteristics of the textured samples were assessed with an optical interferometer model Zygo OMP-0347C. Examples of two patterns containing circles with similar diameters and depths but different percentages of area coverage are shown in Figure 1. The nomenclature used for all the samples tested and average values for the features that compose the textures are presented in Table 2. Some identical samples were produced, but they were tested at different orientations in relation to the sliding direction. The relative orientations between the sliding direction and the geometry of the textures are also presented in this table.

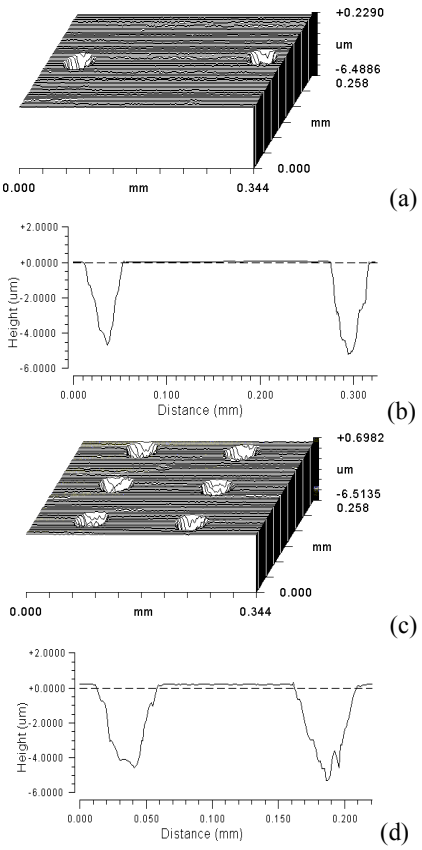

Figure 1. Surface topography of the textured samples; (a) - Sample T1, perpendicular view; (b) - Sample T1, line profile; (c) - Sample T2, perpendicular view; (d) - Sample T2, line profile.

Table 2. Geometric features of the samples; *w* - width of the features; h_1 - depth; *f* - fraction of area coverage.

Name	Shape	*w* (μm)	h_1 (μm)	*f*	h_1/w	Sliding orientation
T1	Circle	41	4.5	0.019	0.11	
T2	Circle	40	4.5	0.049	0.11	
T3	Circle	47	4.5	0.113	0.10	
T4	Circle	70	6	0.15	0.09	
T5	Line	42	4.5	0.15	0.11	
T6	Line	40	4.5	0.238	0.11	
T7	Circle	25	1.8	0.045	0.07	
T8	Line	40	4.5	0.238	0.11	
T9	Line	40	4.5	0.238	0.11	
T10	Chevron	85 x 60 x 35	4.5	0.073	0.12	
T11						

Reciprocating tests were used to evaluate the behaviour of the textured surfaces in lubricated sliding, giving variable sliding velocity during each stroke of the test, which enabled changes in the lubrication regime to be seen in a single test. Sinusoidal linear motion at a frequency of 0.55 Hz was produced by a crank mechanism. The length of each stroke was 22 mm. A mirror-polished, 100 mm diameter sector of an aluminium cylinder slid against the textured steel plates and the contact region was immersed in an oil reservoir. This very large radius was chosen to guarantee large contact widths for this model experiment. A mineral oil without additives and a dynamic viscosity at 20 ^oC of 1.5 Pa s was used. The temperature of the environment was controlled at 20 ^oC. Two crossed cylinders helped to align the normal force, which was applied by dead weights. Different loads were used, in order to vary the contact width. The loads and their corresponding contact widths (*2a),* calculated using the Hertz equation, are presented in Table 3.

Table 3. Normal loads and corresponding elastic contact widths used in the sliding tests.

Load (N)	12.3	22.1	31.9	41.7	51.5	61.3	71.1	80.9
Contact width (μm)	82	111	133	152	169	184	198	212

The variables continuously measured during each test were friction force and film capacitance. The running-in period of the samples was evaluated through observation of the film capacitance during the tests and the data were collected only after a steady lubricant film was observed. This duration depended on the texture on the sample and varied from 1.5 hours to 4 hours. After the running-in period, data for friction and capacitance were acquired for

a total of 150 cycles. The data were digitally sampled using a data acquisition unit (Iotech Datashuttle USB55) with a sampling frequency of 37 Hz. Points in consecutive cycles with the same translational velocity were averaged in order to obtain mean values of friction force and film capacitance for an average stroke as a function of speed. After the tests, the worn surfaces were scanned using a digital optical scanner (HP ScanJet 5300c) to record surface damage features.

3. Capacitance measurements

In lubricated sliding tests of metallic samples, the two samples can be treated as two conductors separated by a lubricant dielectric film, which constitute a capacitor. The value of the capacitance (C) for a cylinder on a plate in a medium of dielectric constant ε depends on the length (l) and radius (R) of the cylinder and the minimum thickness of the dielectric film (h_0), as follows:

$$C = \frac{2\pi\varepsilon\varepsilon_o l}{\cosh^{-1}\left(1+\frac{h_o}{r}\right)} \qquad \text{Eq. 1}$$

However, for a textured surface, this equation must be corrected to take into account the fact that the non-textured and textured portions of the surface are at different distances from the cylinder. A simple approach is to treat it as the summation of two capacitances in parallel, where each is given by:

$$C_{non-text.} = (1-f)*\frac{2\pi\varepsilon\varepsilon_o l}{\cosh^{-1}\left(1+\frac{h_o}{r}\right)}$$

$$C_{text.} = (f)*\frac{2\pi\varepsilon\varepsilon_o l}{\cosh^{-1}\left(1+\frac{h_o+h_1}{r}\right)} \qquad \textbf{Eq. 2}$$

In this work, a specially designed bridge circuit, in which the capacitor created by the two samples and the lubricant film is one of the components, was connected to an AC power supply. Variations in the value of the capacitance upset the balance of the bridge, which was reflected in the voltage signal between points 1 and 4 of the electronic circuit shown in Fig. 2.

The minimum film thickness between a sliding cylinder and a smooth flat surface due to hydrodynamic pressure depends on the viscosity of the lubricant (η), the normal load (P), the velocity (U) and the length (L) and radius (R) of the cylinder, as given by [13]:

$$h_o = \frac{4.89\eta RUL}{P} \qquad \textbf{Eq. 3}$$

This equation was used to make estimate the range of minimum film thicknesses expected depending on the geometry of the samples, the loads to be used and the velocities at the middle of the stroke. Then, using Eq. 1, the relevant range of capacitances for the tests was calculated to lie between 50 and 900 pF. These values guided the choice of the resistors that compose the bridge, which were chosen in order to provide a fairly linear variation between the capacitance and the corresponding voltage signal for this range of capacitances.

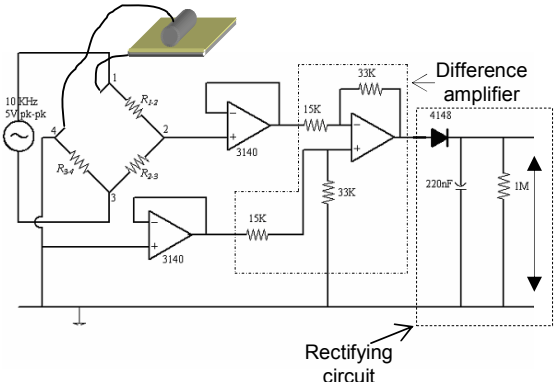

Figure 2. Complete electronic circuit used to measure capacitance in the sliding tests.

The output from the sliding tests was a sequence of DC voltage measurements over time, corresponding to the average of the AC signal for the film thickness at each point of the stroke. After calibration, the output values could be plotted as a sequence of capacitance values over time. Figure 3a shows an example of a plot of this sequence for sample T2, at a normal load of 61.3 N, between 149 and 154 s. For comparison, the friction force signal is also presented. It can be clearly seen that both friction and capacitance follow a pattern that is repeatedly cyclic, corresponding to each stroke of the reciprocating test. The points corresponding to zero force are the reversal points of the strokes. The speed within each stroke varies sinusoidally from zero at the reversal points to a maximum value at the middle of the stroke. It is then interesting to compute an average stroke, which corresponds to an average of all the corresponding points inside each stroke along the whole length of the test. For example, the mean friction $\overline{F}$ for the point A in the average stroke, shown in Figure 3b, which is at a distance t_1 from the point where the friction force changes its sign (zero force) is given by $\overline{F} = \left[\sum_{i=1}^{n} F(A_i)\right]/n$, where A_i are the points in consecutive strokes at a distance t_1 from the point where the friction force changes its sign for each cycle and n is the number of cycles. However, it must be pointed out that, even after the running-in period, occasional disturbances in the capacitance signal were observed, which were believed to correspond to points where metallic wear debris was entrapped in the contact, resulting in contact between the sliding surfaces and

consequently very low capacitance, as exemplified in Fig. 3c. This hypothesis was strengthened by the fact that the presence of those disturbances was mainly restricted to the higher normal loads and was not observed for the four lowest loads. Also, the presence of very occasional scratches observed in the worn samples extending for the whole length of the stroke might also suggest occasional entrapping of wear debris in the contact, although most of the wear damage was concentrated very close to the extremes of the stroke. The cycles for which this happened were eliminated from the averaging analysis. After the average stroke was computed using the methodology just described, Equation 2 was used to compute the minimum film thickness h_o from the capacitance values, which is shown as a function of the instantaneous sliding velocity in Fig. 3d.

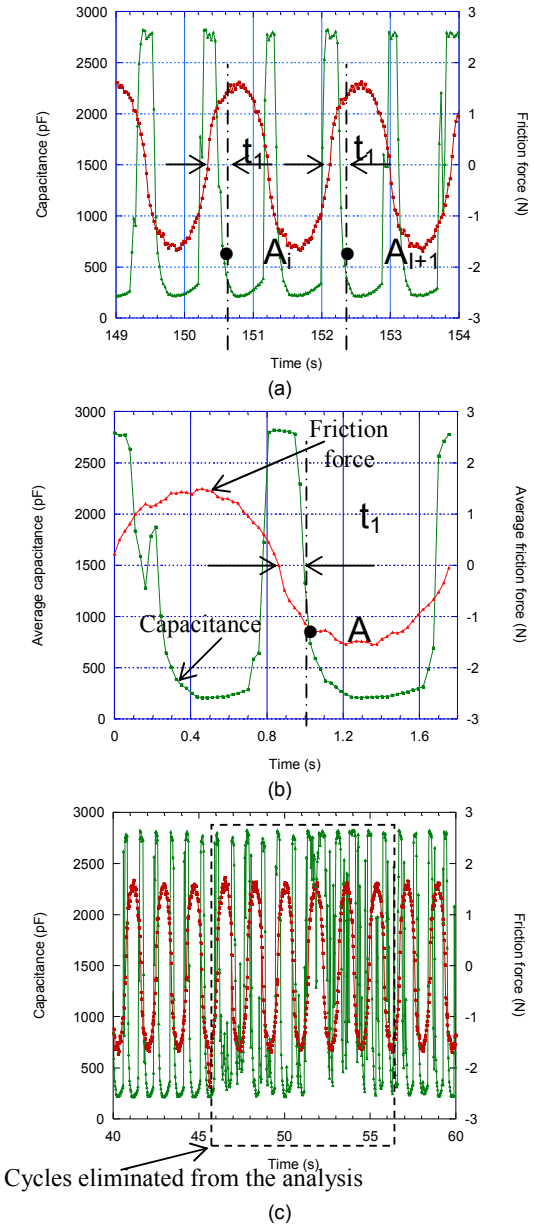

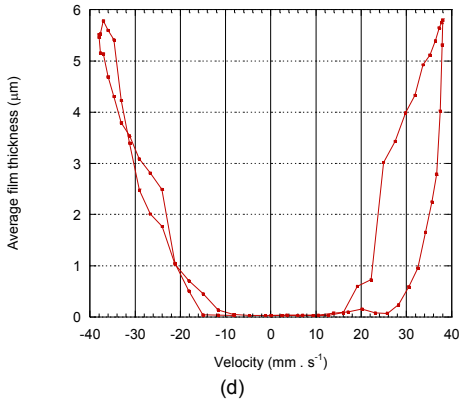

Figure 3. Methodology for the data analysis, using as an example sample T2 at a load 0f 61.3 N; (a) - a sequence of cycles, which are averaged to calculate (b) - the average stroke; (c) - a sequence of cycles with some cycles presenting a disturbance in the capacitance signal; (d) - estimation of the film thickness as a function of the sliding velocity for the average stroke.

Fixed capacitors were used to calibrate the circuit. The experimental calibration curve is compared to the theoretical curve obtained from an analytical model of the bridge performance in Fig. 4.

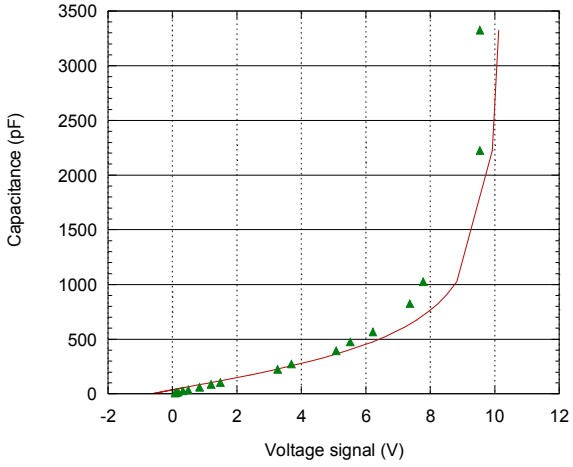

Figure 4. Comparison between the calibration curve using fixed capacitors (triangular points) and the calculated correlation between the voltage signal and the capacitance (line).

4. Results

Fig. 5 presents, as an example, images of two of the worn surfaces after the sliding tests. Similar features were observed for all the samples tested.

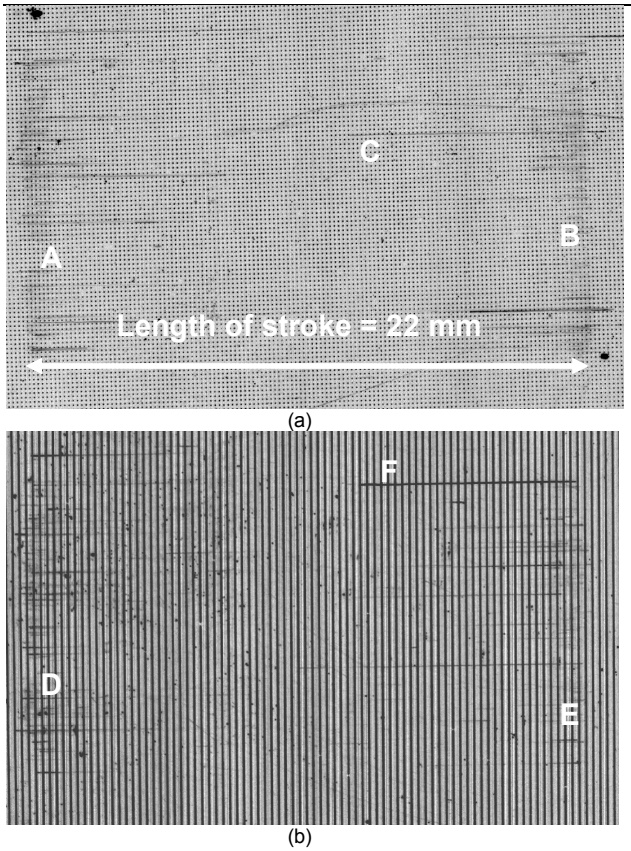

Figure 5. Examples of features on worn surfaces after the sliding tests; (a) - sample T2; (b) - sample T5; A, B, D and E indicate the areas where most of the wear damage occurred; C and F indicate occasional scratches across the stroke.

The effect of the texturing of the surfaces was analysed for different loads. An example of the effect of fraction of area coverage for samples containing circular features on film thickness and friction force for a load of 51.5 N is shown in Fig. 6.

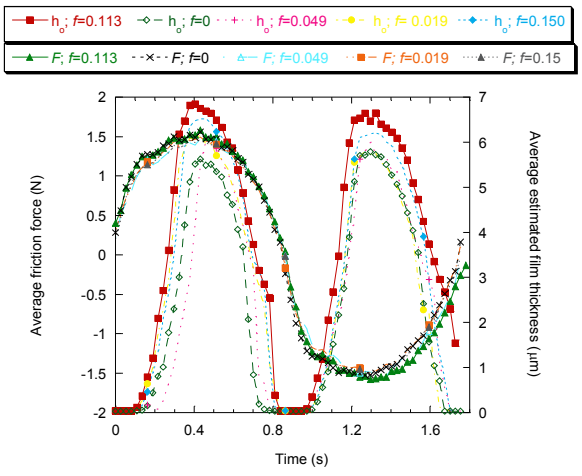

Figure 6. Comparison of friction force and film thickness for averaged strokes for samples textured with circular features at different fractions of area coverage for a load of 51.5 N.

The effects of the variables involved in the texturing on the film thickness were considered individually. These variables were the fraction of area coverage, the size of the features, the effect of direction and the shape of the features. To carry out these analysis, the values of minimum film thickness h_o, obtained at the middle of the average stroke, where the highest value for h_o is obtained, were plotted against the normal load.

The effect of coverage fraction is shown in Fig. 7 for different loads, for patterns containing circular pockets and lines. Samples sliding with different orientations between the sliding direction and the geometry of the pattern are compared in Fig. 9, both for patterns containing lines (Fig. 9a) and chevrons (9b). The effect of the shape of the features that compose the pattern (circles, lines or chevrons) was compared in Fig. 9.

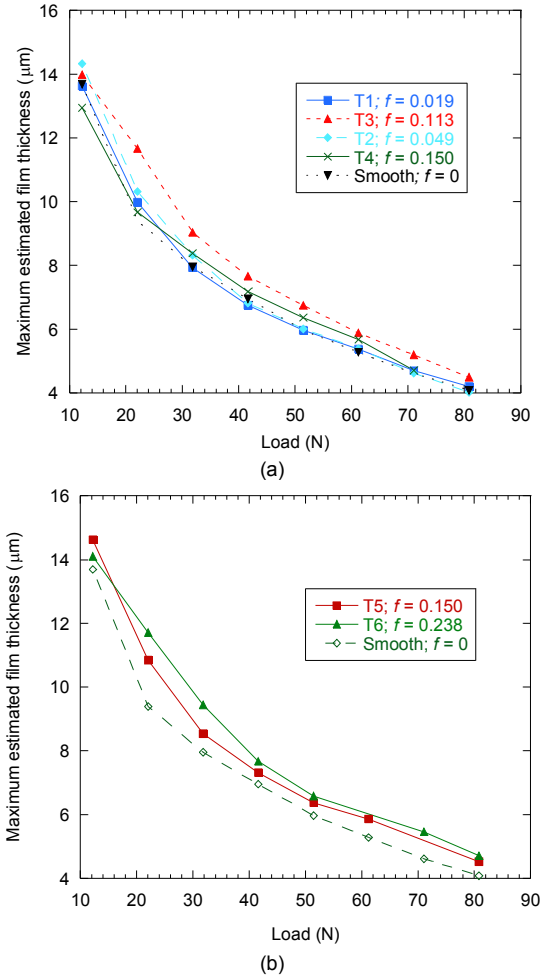

Figure 7. Effect on maximum film thickness of the area coverage fraction f for various loads; (a) - patterns containing circular features; (b) - patterns containing lines oriented perpendicular to the sliding direction.

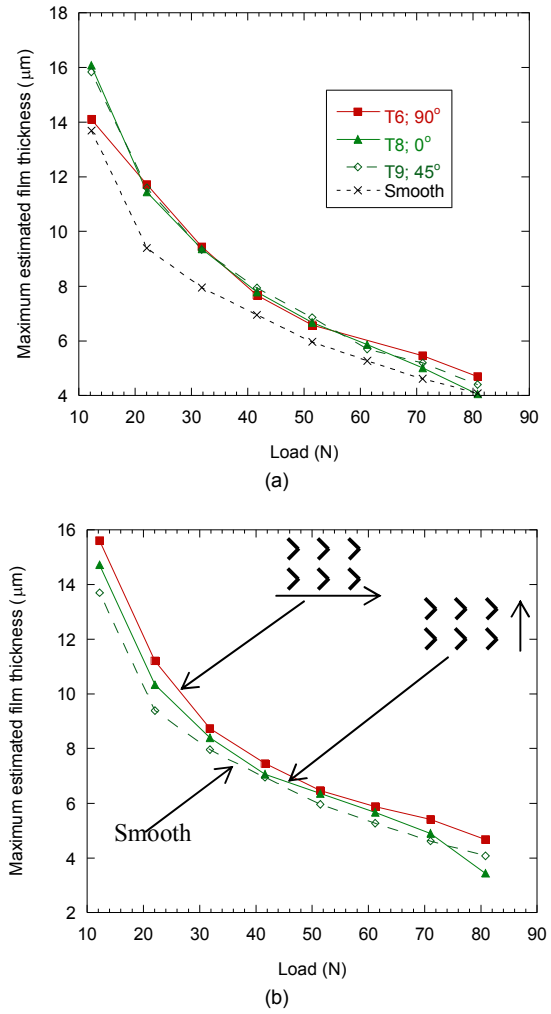

Figure 8. Effect on maximum film thickness of the relative orientation between the sliding direction and the surface features for various loads; (a) - lines; (b) - chevrons.

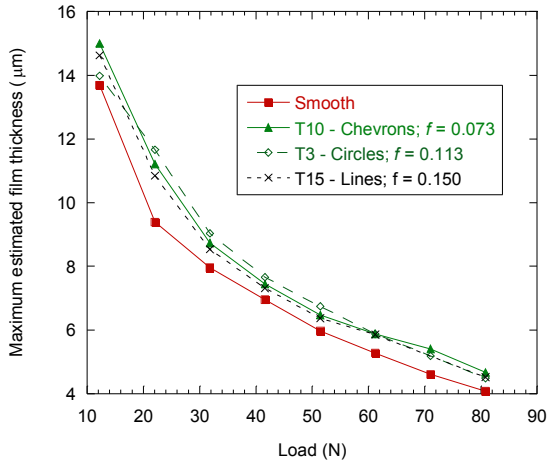

Figure 9. Effect on maximum film thickness of the shape of the features that compose the texture for different normal loads.

5. Discussion

For the calibration curves presented in Fig. 4, there is a discrepancy between the actual values of the fixed capacitances used in the calibration process and the values calculated analytically, for capacitances corresponding to voltage signals smaller than zero, since the rectifier portion of the circuit does not allow measurement of negative voltages. For capacitances that correspond to positive voltage signals, there is fairly good agreement between the calculated and measured values. An interpolation curve fit was applied to the experimental calibration data to convert to voltage signal values into capacitance, in order to achieve higher accuracy of the results.

As seen in Fig. 6, the friction coefficient curves present an approximately sinusoidal shape, in the same way as the variation of the instantaneous velocity along the strokes. This suggests that for the majority of the length of the stroke, a hydrodynamic or full film lubrication regime is present, as predicted from the Stribeck curve [14]. This hypothesis is confirmed by the worn surfaces exemplified in Fig. 5, which shows that most of the wear is concentrated at the extremes of the stroke, and that virtually no wear is observed for the majority of the length of the stroke. A few rare scratches cross the whole length of the stroke and, according to the argument presented during the description of the capacitance measurements, they must be associated with occasional wear debris particles becoming entrapped between the sliding surfaces. From Figure 6 it is also possible to observe that the variation of the area coverage fraction does not reflect in variation in the friction force curves. This behaviour is in accordance with the results obtained by Petterson and Jacobson [10], who analysed the effect of shape, size and orientation of textured surfaces on the friction of lubricated textured surfaces using ball-on-flat reciprocating tests. When boundary lubrication conditions were used, the texturing of the surfaces resulted in variation in the friction coefficient for some sliding configurations. However, when an ample amount of oil was supplied, the friction was rather insensitive to the texturing for all the configurations. This behaviour was believed to be due to an adequate amount of lubricant being present for all the configurations anyway, even without the texturing.

On the other hand, significant changes in the film thickness can be seen in Fig. 6, due to the texturing of the surfaces. For all the configurations analysed, the texturing of the surfaces never resulted in changes in the friction force, but for some of them significant variations in the film thickness were observed. For this reason, the analysis carried out in this work was based on the film thickness measurements. However, the friction force measurements were necessary to help to identify the beginning and end of each stroke, since they were the points corresponding to zero friction force.

For samples with circular pockets, a maximum was observed in the relationship between the area coverage fraction and film thickness, as Fig. 7a evidences. Although the samples have different values of w and h_1,

all of them have similar h_1/w ratios of around 0.1, which is regarded in the literature as the main non-dimensional parameter of the texture that describes the size of the features [5, 8, 9, 15]. For sample T1, with a very low area coverage fraction of 0.019, there was virtually no difference between textured and smooth samples. A small increase in the film thickness was observed for sample T2, with f = 0.045. The maximum increase in film thickness was observed for the sample T3, with an area coverage fraction of 0.113. The increase in film thickness for the sample T4, with f = 0.150 was smaller than that for sample T3. This suggests that there is a limit to the increase of performance with fraction of texturing, after which its effect might be counterbalanced by the reduction in the contact area. For very low loads, where the contact width was narrower, the increase in the performance of the textured surfaces in relation to the smooth sample was always much less significant than for the other loads. This difference was more pronounced for the sample with larger pockets (T4). For the samples with lines, the film thickness increased when the area coverage fraction increased from zero to 0.150 and then 0.238 and no maximum was observed within this range, as can be seen in Figure 7b.

Brizmer et al. [6] found a linear relationship between area coverage fraction and the load capacity of parallel thrust bearings when they used finite differences to discretize the Reynolds equation for sliders with textured surfaces with appropriate boundary conditions, instead of a maximum. They analysed the effect of the texturing parameters on the load carrying capacity of bearing surfaces both fully textured and with a portion of their length textured. However, Mitidieri [7] suggests an optimum behaviour for bearings with an area coverage fraction of 0.25, based on modelling of hydrodynamic bearings containing small cavities using computational fluid dynamics. Wang et al. [8] found a maximum in the correlation between area coverage and load capacity in their experiments, but the optimum point occurred for a smaller area coverage fraction. They used disk-on-cylinder tests under water lubrication to analyse the effect of laser texturing on the lubrication regime transition for SiC samples. Increasing loads were used and the load for which there was a sharp increase in the coefficient of friction was defined as the transition load between hydrodynamic lubrication and mixed lubrication. The optimum percentage of area coverage was found to be 2.8% and, for percentages of coverage higher than 7%, the critical load of the textured surfaces was lower than that of the non-textured surfaces. Later, these authors extended the study to SiC surfaces textured by ion reaction etching (IRE), with a larger range of textured conditions [9]. The results obtained in this extended study for conditions with plentiful supply of lubricant water showed an optimum percentage of coverage of around 5%.

Fig. 8a shows that the effect of the relative orientation between the sliding direction and the texture was not significant for the samples patterned with lines for loads between 22.1 and 61.3 N. For the lowest load of 12.3 N, the sample with lines oriented perpendicularly to the sliding direction (T6) presented a worse behaviour than the other two textured samples. The samples patterned with circles presented a similar behaviour to sample T6 when sliding at load of 12.3 N. It can be suggested that for this narrow contact width, not many 'pockets' are present inside the contact zone to increase the hydrodynamic pressure. This effect was probably not observed for the other two directions because the lines were oriented in relation to the contact width in such a way that there was still a considerable proportion of textured area within the contact width even when the contact width was narrower. For the higher normal loads of 71.1 and 80.9 N, the sample with lines perpendicular to the sliding (T6) presented the highest film thickness, then followed by the sample with lines at 45^o (T9) and then the samples with lines parallel to the sliding (T8). This effect could be due to a tendency of the lines to channel the lubricant away from the contact the more they are oriented in the direction of the sliding. This effect should be more significant for higher normal loads.

The samples patterned with chevrons presented different behaviours when the relative orientation between the chevrons and the sliding direction was changed, for the whole range of loads tested, as is clearly seen in Fig. 8b. When the corners of the chevrons were oriented in the direction of the sliding, there was a significant increase in the film thickness. However, when they were oriented perpendicular to the sliding, the increase in film thickness was smaller for all the loads tested. Also, for the highest normal load of 80.9, the sample with the chevrons oriented perpendicular to the sliding showed behaviour even worse than that of the smooth surface. Again, some channelling of the lubricant away from the contact for higher loads might occurs. This effect did not happen when the chevrons were parallel to the sliding.

The samples patterned with different shapes shown in Fig. 9 presented very similar increases in the film thickness in relation to the smooth sample. However, the area coverage fraction was the smallest for the sample containing chevrons (0.073) and the highest for the samples containing lines (0.238). This might suggest that the chevrons are a more efficient shape when an increase of hydrodynamic film thickness is sought. Stachowiak proposed a similar macrogeometry for a hydrodynamic bearing with improved performance, with the chevrons oriented in the direction of sliding [16]. Lines could also be regarded as the least efficient shapes to increase the hydrodynamic pressure. This could be related to the hypothesis of the lines channelling the lubricant away from the contact, as also suggested by Steinhoff et al. [3] via study of the effect of surface texturing in situations involving intense plastic deformation.

5. Conclusions

- The measurement of film capacitance was shown to be a suitable technique to evaluate the effect of surface texturing on lubrication under conditions of a plentiful supply of oil. Certain patterns of surface texturing were efficient increasing the lubricant film thickness.
- For patterns containing circular pockets, there was a maximum in the correlation between the area coverage

fraction of the pattern and the film thickness. For very low area coverage there was no effect on the film thickness. For patterns containing lines an increase in the area coverage resulted in an increase in the film thickness, for the two different area coverages tested.

- All the samples with patterns containing circular pockets or lines perpendicular to the sliding direction had a much smaller effect on the film thickness for narrower contact widths. This effect was more significant for the sample with larger pockets.
- For intermediate loads, there was no effect on the film thickness of the orientation of the lines relative to the sliding direction. For the smallest normal load of 12.3 N the sample with lines perpendicular to the sliding had the lowest film thickness. For the two higher loads of 71.1 and 80.9 N, the best behaviour was for sliding perpendicular to the lines, followed by the sample with lines at 45^{o} and then by the sample with lines parallel to the sliding direction.
- The sample with chevrons oriented parallel to the sliding direction gave higher film thicknesses than a sample sliding in a perpendicular direction for all the loads tested.
- Chevrons seem to be the most efficient shape for the features that compose the pattern, and lines the least efficient, when an increase of hydrodynamic film thickness is sought.

6. Acknowledgements

The authors acknowledge Alan Thorne for technical support with the capacitance measurements and CAPES/Brazil for financial support.

7. References

1. Becker, E.P. and K.C. Ludema, *A qualitative empirical model of cylinder bore wear.* Wear, 1999. **225-229**: p. 387-404.
2. Dubrujeaud, B., M. Vardavoulias, and M. Jeandin, *The role of porosity in dry sliding wear of a sintered ferrous.* Wear, 1994. **174**: p. 155-161.
3. Steinhoff, K., W. Rasp, and O. Pawelski, *Development of deterministic-stochastic surface structures to improve the tribological conditions of sheet forming processes.* Journal of Materials Processing Technology, 1996. **60**: p. 355-361.
4. Hamilton, D.B., J.A. Walowit, and C.M. Allen, *A theory of lubrication by micro-irregularities.* Transactions of ASME, Journal of Basic Engineering, 1966: p. 177-185.
5. Ronen, A., I. Etsion, and Y. Kligerman, *Friction-reducing surface-texturing in reciprocating automotive components.* Tribology Transactions, 2001. **44**(3): p. 359-366.
6. Brizmer, V., Y. Kligerman, and I. Etsion, *A laser surface textured parallel thrust bearing.* Tribology Transactions, 2003. **46**(3): p. 397-403.
7. Mitidieri, P.B. *CFD modelling of a low friction hydrodynamic bearing*. in *Tribology Mission*. 2002. London: IMechE.
8. Wang, X., et al., *The effect of laser texturing of SiC surface on the critical load for the transition of water lubrication model from hydrodynamic to mixed.* Tribology International, 2001. **34**: p. 703-711.
9. Wang, X., K. Kato, and K. Adachi, *The lubrication effect of micro-pits on parallel sliding faces of SiC in water.* Tribology transactions, 2002. **45**(3): p. 294-301.
10. Pettersson, U. and S. Jacobson, *Friction and wear properties of micro textured DLC coated surfaces in boundary lubricated sliding.* Tribology letters, 2004. **17**(3): p. 553-559.
11. Madou, M.J., *Fundamentals of Microfabrication*. 2nd ed. The Science of Miniaturization. 2002, Florida: CRC Press. 723.
12. Cochran, D.A., *Apparatus and method for electrochemically etching grooves in an outer surface of a shaft*, in *USPTO*. 2001, Seagate Technology: United States.
13. Williams, J.A., *Engineering Tribology*. 1994, Oxford: Oxford University Press. 488.
14. Hutchings, I.M., *Tribology - Friction and Wear of Engineering Materials*. 1992, London: Arnold. 273.
15. Etsion, I., Y. Kligerman, and G. Halperin, *Analytical and experimental investigation of laser-textured mechanical seal faces.* Tribology Transactions, 1999. **42**(3): p. 511-516.
16. Stachowiak, G.W. and A.W. Batchelor, *Engineering Tribology*. 2001, Boston: Butterworth-Heinemann. 744.